Journal of Power Sources 255 (2014) 116–124

Contents lists available at ScienceDirect

Journal of Power Sources

journal homepage: www.elsevier.com/locate/jpowsour

Laser-printing and femtosecond-laser structuring of $LiMn_2O_4$ composite cathodes for Li-ion microbatteries

J. Pröll [a,*], H. Kim [b], A. Piqué [b], H.J. Seifert [a], W. Pfleging [a,c]

[a] Karlsruhe Institute of Technology, Institute for Applied Materials, P.O. Box 3640, 76021 Karlsruhe, Germany
[b] Naval Research Laboratory, Washington DC 20375, USA
[c] Karlsruhe Nano Micro Facility, Hermann-von-Helmholtz-Platz 1, 76344 Eggenstein-Leopoldshafen, Germany

HIGHLIGHTS

- Combination of laser-printing and 3D laser structuring of porous electrodes.
- Reduced electrochemical degradation and improved cell kinetic for structured cathodes.
- Calendered/structured cathodes lead to improved cell performance at 1 C discharge.

ARTICLE INFO

Article history:
Received 15 October 2013
Received in revised form
2 December 2013
Accepted 31 December 2013
Available online 8 January 2014

Keywords:
Laser direct-write
Laser-printing
Femtosecond-laser structuring
Lithium-ion battery
Lithium manganese oxide
3D microbattery

ABSTRACT

Porous $LiMn_2O_4$ thick-film cathodes for Li-ion microbatteries are realized by laser-printing. The porous structure of the printed composite cathode consisting of active powder, binder, carbon black and graphite enables ionic and electronic transport through 50–60 μm thick electrodes due to its high intrinsic active surface area. In order to further improve the cycle stability and capacity retention of the laser-printed thick-film cathodes for discharging rates up to 1 C, laser-printed thick films are first calendered in a press and then structured using ultrafast femtosecond-laser radiation in order to form three-dimensional (3D) cathode architectures. It is shown that calendered/laser structured cathodes in the form of rectangular 3D grids exhibit discharge capacity retention of 68% at a 1 C rate, while calendered but unstructured cathodes retain only about 45% of their initial capacity at the same discharge rate. Overall, the improved discharge capacity retention and reduced degradation during later cycles can be attributed to the combination of increased electrical contact with shortened Li-ion pathways.

1. Introduction

Lithium manganese oxide ($LiMn_2O_4$) is a promising cathode material for Li-ion batteries due to its high theoretical capacity of 148 mAh g^{-1} [1], its low cost and environmental friendliness [2], especially for applications requiring Li-ion microbatteries as in micro-electronic devices [3] or micro-electromechanical systems [4]. Besides conventional coating routes for active materials in the form of compact thin films using radio frequency sputtering [5] or porous thick films by tape casting [6], $LiMn_2O_4$ has also been laser-printed for the fabrication of Li-ion microbatteries using a laser direct write (LDW) technique [7]. LDW is suitable for printing of numerous complex materials such as single- or multi-component systems used as electrochemical materials [8] as well as for micromachining defined shapes for current collectors onto which inks containing active battery materials, e.g. lithium cobalt oxide ($LiCoO_2$), were laser-printed by LDW [9]. This technique can be used for printing of thick-film electrodes or even complete solid-state microbatteries which show improved electrochemical properties compared with those prepared by sputter-deposited thin-film techniques [3]. The LDW technique allows for manufacturing highly porous composite cathodes containing active particles, binder, and carbon black with adjustable thickness to overcome the limitations of internal cell resistance of sputtered thin-film cathodes. Furthermore, LDW can be combined with subsequent laser structuring in order to form conical microstructures for further increase of active surface area [10]. In fact, three-dimensional (3D) microbattery architectures are generating great interest since they can achieve large areal energy capacities, while maintaining high power densities [11].

Additionally, laser structuring has been shown to be a powerful technique for stabilizing the capacity retention of thin film

* Corresponding author.
E-mail address: johannes.proell@kit.edu (J. Pröll).

0378-7753/$ – see front matter © 2014 Elsevier B.V. All rights reserved.
http://dx.doi.org/10.1016/j.jpowsour.2013.12.132

electrode materials such as $LiCoO_2$, tin oxide and $LiMn_2O_4$ by increasing the active surface area thus improving Li-ion diffusion out of compact films with thicknesses of 2–3.5 μm, as well as for building-up 3D thin film cell designs [12–16]. Three-dimensional conical microstructures can be generated in thin films by direct ablation or by a self-organizing effect. For example, the formation of conical microstructures has been observed after laser irradiation of tape-casted electrodes [17]. This paper will discuss how to manufacture 3D cathode architectures by applying an ultrafast laser ablation process on laser-printed electrodes. The results for several arrangements of laser-printed $LiMn_2O_4$ thick-film cathodes such as calendered, laser structured and calendered/structured films will be presented and compared to untreated films. Calendering of laser-printed films was investigated due to the fact that calendering techniques are usually applied for tape-casted and slurry-based electrodes in lithium-ion batteries leading in general to an enhancement of power density and film adhesion as well as allowing control of intrinsic porosity. Subsequent processing into 3D grid microstructures via femtosecond (fs)-laser structuring further increased the active surface of the cathodes without compromising their electrical contact. The impact of these modifications and their combinations on the electrochemical behaviour will be analysed. Finally, the findings within these investigations will help determine optimized processing conditions for combination of laser-printing and ultrafast laser structuring of porous multi-material compositions for development of long life-time 3D microbatteries.

2. Experimental

2.1. $LiMn_2O_4$ cathode material

The cathode ink was prepared by mixing 90 wt.% $LiMn_2O_4$ (Aldrich), 4 wt.% graphite (KS6, Timcal) and 2 wt.% carbon black (Super P, Erachem) in a solution of 4 wt.% PVDF-HFP (Kynar 2801, Elf Atochem) in dibasic ester (DBE, Du Pont) solvent. The cathode inks were laser-printed onto 50 μm thick aluminium (Al) current collectors. In the electrode formulation, the graphite (KS6) was added to improve the electric conductivity and the carbon black (Super P) was added to increase porosity in the electrode films. The PVDF-HFP was used as a binder to hold the electrode films onto current collectors. The DBE was selected because it is a good solvent for PVDF binder and its boiling temperature is relatively high (~210 °C) [3].

2.2. Laser-printing process

The laser-printing process used in this work has been described in detail elsewhere [3]. Briefly, a small amount of ink formulation was uniformly spread using a wire coater (#5, Garner) onto a 7.5 cm diameter UV transparent quartz wafer (this ink-coated wafer is also referred to as the ribbon). A vacuum chuck on top of the X–Y stages was used to secure both the substrate and ribbon. For the laser-printing of the cathode ink, a frequency-tripled Nd:YVO_4 (JDSU, Q301-HD) pulsed laser (λ = 355 nm, 30 ns FWHM) operating at 30 kHz was employed to irradiate ink materials from the ribbon. The energy of the laser pulse was controlled with an acousto-optic modulator inserted into the beam path. For fast printing process a beam scanning system was used. In this arrangement the Al substrate was fixed, while the laser beam was displaced in a raster pattern with a galvo scanner (SCANLAB, intelliSCAN 10). The laser fluence is maintained at ~50 mJ cm^{-2}, while the number of transfer passes is varied to control the transferred film thickness. Once laser-printed, the electrodes were dried in a vacuum oven at 120 °C for 24 h in order to remove the DBE solvent and any absorbed water.

2.3. Laser structuring process

Microstructures were formed in laser-printed $LiMn_2O_4$ thick films by using fs-laser radiation. Laser structuring was performed using a micromachining workstation (PS450-TO, Optec, Belgium) equipped with a tunable fiber laser (Tangerine, Amplitude Systemes, France) with an average power of 20 W and a maximum pulse energy of 100 μJ at 1030 nm (TEM_{00} with $M^2 < 1.3$), a variable pulse repetition rate of up to 2 MHz and tunable laser pulse duration from 330 fs up to 10 ps. Second harmonic (SHG) and third harmonic generation (THG) efficiency was specified to be >40% and >15% at 200 kHz, respectively (Fig. 1).

The structuring process was performed for all samples applying a laser wavelength of 515 nm, a repetition rate of 200 kHz, a laser power of 25 mW at the sample surface and a pulse duration of about 350 fs. Furthermore, the structuring process was carried out under ambient air, and the ablated material was removed by an exhaust.

By applying a power of P = 25 mW and a repetition rate of f = 200 kHz, the pulse energy was calculated to be E_p = 0.125 μJ. This equals a pulse peak power of $P_P = 3.57 \times 10^5$ W and an intensity of $I = 5.6 \times 10^{10}$ W cm^{-2} being available for ablating the composite material. The laser pulse overlap Δx was determined to be Δx = 0.5 μm resulting in ~57 laser pulses per irradiated area. For patterning of an area of 1.131 cm^2, the laser beam was scanned over the sample surface using a Rhothor™ Laser Deflection Systems scan head (Newson Engineering BV). The structuring process was performed by scanning the laser beam along each line twice for un-calendered films and four times for calendered films as indicated in Fig. 2. The scanning velocity was set to v = 100 mm s^{-1} for all experiments.

2.4. Calendering process

Laser-printed thick-film cathodes were optionally pressed before the structuring process in order to achieve uniform film thickness over the substrate area and improved electrical contact of $LiMn_2O_4$ particles to the Al substrate. A compact hot rolling press (Precision 4″ Hot Rolling Press/Calender, MTI Corporation, USA) equipped with heatable rolls (100 mm diameter, 100 mm width) was used with adjustable roller distance ranging from 0 mm to 1.2 mm and adjustable rolling speed ranging from 0 mm s^{-1} to 40 mm s^{-1}. Laser-printed thick films were calendered in order to achieve overall film thickness of about 100 μm including thickness of the film and Al substrate. For each sample and roller distance, the calendering process was repeated up to five times to counter thickness relaxation of the composite electrode after passing the rollers. The rolling speed was set to 8 mm s^{-1} and the roller temperature was maintained at 53 °C.

2.5. Electrochemical characterization

Laser-printed, calendered, and laser structured $LiMn_2O_4$ thick films were electrochemically tested using a Swagelok® cell design.

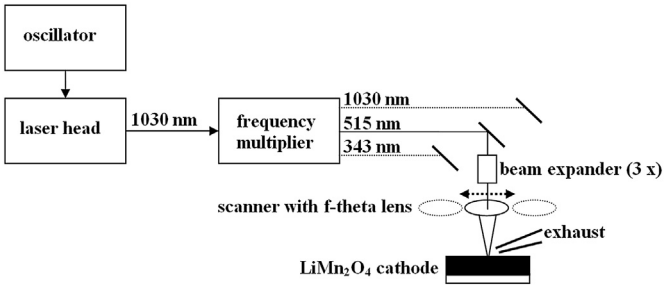

Fig. 1. A schematic diagram of the laser micromachining system.

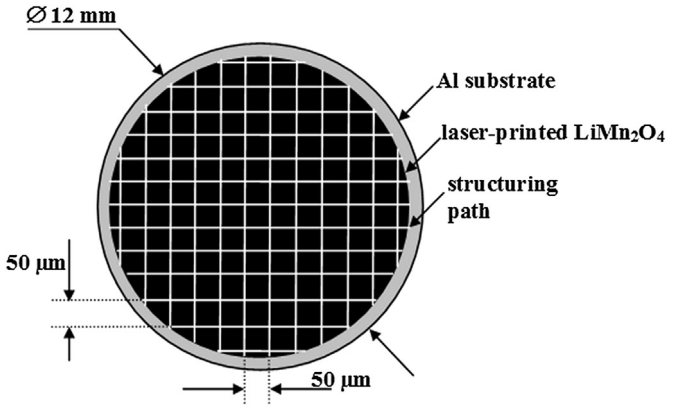

Fig. 2. Schematic diagram of a laser-printed and laser structured $LiMn_2O_4$ thick film for achieving 3D grid microstructures.

The basic set-up of the test cell is described elsewhere [10]. Swagelok® cells were assembled for both galvanostatic and cyclic voltammetric (CV) measurements in an argon-filled glove box (LABmaster sp, M. Braun Inertgas-Systeme GmbH) with $H_2O < 0.1$ ppm and $O_2 < 0.1$ ppm. Metallic lithium foil was used as counter electrode. The electrolyte was LP30 (Merck AG) consisting of a mixture of ethylene carbonate and dimethyl carbonate (EC/DMC 1:1) with 1 M lithium hexafluorophosphate (1 M $LiPF_6$) conducting salt. The amount of electrolyte used for one cell was 100 µl. The separator was a glass microfibre with a thickness of 260 µm (GF/A filter, Whatman company). CV and galvanostatic testing were performed using an Arbin Instruments BT2000 battery cycler. Electrochemical priming was carried out for three cycles by CV measurements in a voltage window of 3.0–4.3 V and a constant 0.02 mV s^{-1} scan rate resulting in charging and discharging times of about 18 h for each half-cycle. The available capacity was measured out of the 3rd CV cycle and was used for C-rate calculation for further galvanostatic testing in the voltage window of 3.0–4.2 V. The galvanostatic testing procedure was as follows (Table 1): Charging and discharging with C/10 for five cycles, charging and discharging for 10 cycles with C/5, charging with C/5 and discharging with C/2 or 1 C, each for 10 cycles. Irreversible capacity loss was measured by reducing the charging and discharging rate to C/5 for further 10 cycles.

After galvanostatic cycling, the electrochemical reversibility of untreated, calendered, structured and calendered/structured $LiMn_2O_4$ thick films was investigated by CV scans in the voltage range of 3.0–4.3 V, while the 0.02 mV s^{-1} scan rate was fixed for three cycles and then continuously enhanced by 0.02 mV s^{-1} per cycle up to 0.22 mV s^{-1}.

3. Results and discussion

Within this section, the experimental results for post-treatment of laser-printed $LiMn_2O_4$ thick films are presented. Fig. 3 illustrates the various battery arrangements and corresponding processing procedure for each film/treatment combination and electrochemical testing protocol in the form of a flow-chart.

In a first step, laser-printed (untreated) and various types of modified thick films (calendered, laser structured and calendered/structured) were electrochemically cycled using the cyclic voltammetry method (Fig. 3). In a second step, galvanostatic C-rate testing was applied for evaluating the high C-rate behaviour and coulomb efficiency for each battery arrangement. Finally, cyclic voltammetry measurements were performed using variable scan rate for testing reversible extraction and insertion processes of Li-ions for each battery arrangement after C-rate variation.

Table 1
Galvanostatic testing procedure for Swagelok® cells with untreated and laser modified $LiMn_2O_4$ thick films.

C-rate (charge)	C/10	C/5	C/5	C/5	C/5
C-rate (discharge)	C/10	C/5	C/2	1 C	C/5
Cycle number	5	10	10	10	10

3.1. Laser-printed $LiMn_2O_4$ thick films

Fig. 4 shows SEM images from the top-view of a typical laser-printed $LiMn_2O_4$ cathode film. The $LiMn_2O_4$ particle size is estimated to be in the range of 500 nm to 3 µm (Fig. 4, b). As shown by the SEM micrographs, the $LiMn_2O_4$ particles are interconnected (Fig. 4, a) and carbon black/graphite and binder coat the particles homogeneously (Fig. 4, b) for electrical contact through the cathode film while the particles embedded into the binder matrix form a flexible and mechanically reinforced cathode film. Laser-printed $LiMn_2O_4$ thick films of this type were used for subsequent modification such as calendering, laser structuring or combination of both techniques as described in Fig. 3.

3.2. Laser structured $LiMn_2O_4$ thick films

The microstructures formed after fs-laser structuring for un-calendered and calendered $LiMn_2O_4$ thick films are shown in Fig. 5. Three-dimensional grid microstructures could be achieved by laser ablation using the laser scanning strategy shown in Fig. 2 for both un-calendered and calendered $LiMn_2O_4$ thick films. Laser structuring of un-calendered and calendered cathodes corresponds to the modified films described in terms of “laser structured” and “calendered/structured” within Fig. 3. The mass loss after structuring including active material, carbon black, graphite and binder was measured to be 13–15 wt.% for un-calendered and 16–17 wt.% for calendered thick films. Differences in mass loss between un-calendered and calendered films were found in the laser process and the texture of the composite cathode itself before and after calendering was evaluated. After the calendering process, the $LiMn_2O_4$ particles become further mechanically attached by the binder matrix compared to particles in an un-calendered film. The laser scanning strategy was performed four times for calendered films and two times for un-calendered films for achieving material removal down to the substrate. Vaporization of the binder matrix can successfully support the ablation process as was reported by Slocombe et al. [18,19] for ablation of metal/polymer composites, and this effect is more substantial for un-calendered films resulting in higher ablation rates. By taking into account the laser pulse overlap of $\Delta x = 0.5$ µm, the theoretical focus diameter of about 28.4 µm as well as the number of repetitions of the scanning procedure, the composite material could be ablated down to the substrate using ~114 laser pulses per irradiated area for an un-calendered film and ~228 laser pulses for a calendered cathode film. With respect to a film thickness of about 60 µm for an un-calendered film, the mean ablation rate per pulse could be calculated to be ~0.52 µm per pulse. The ablation rate for a calendered cathode with film thickness of about 50 µm is ~0.22 µm per pulse, indicating that the ablation efficiency is enhanced for an un-calendered cathode film.

Nevertheless, calendering is necessary for further improvement of electrical contact as well as for achieving homogeneous film thickness. To further understand the impact of calendering and 3D grids on the electrochemical behaviour of laser-printed $LiMn_2O_4$ thick films, a schematic of the 3D structures was developed for an un-calendered and structured film (Fig. 6, b) by extracting data

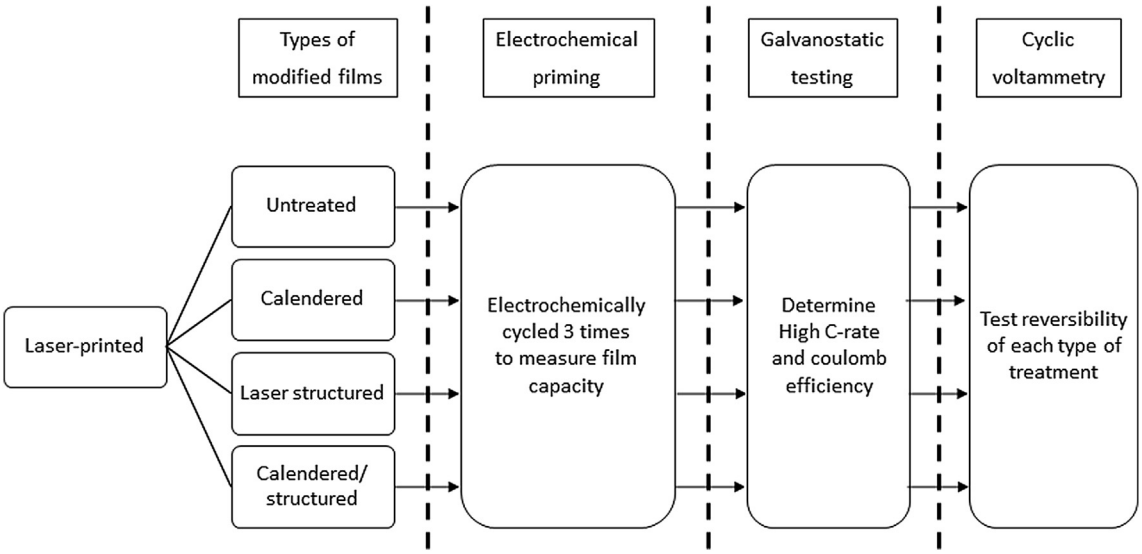

Fig. 3. Flow-chart demonstrating the procedure for experimental investigations of laser-printed $LiMn_2O_4$ thick films: modification of laser-printed films, electrochemical priming by CV formation, galvanostatic testing and CV cycling for reversibility tests.

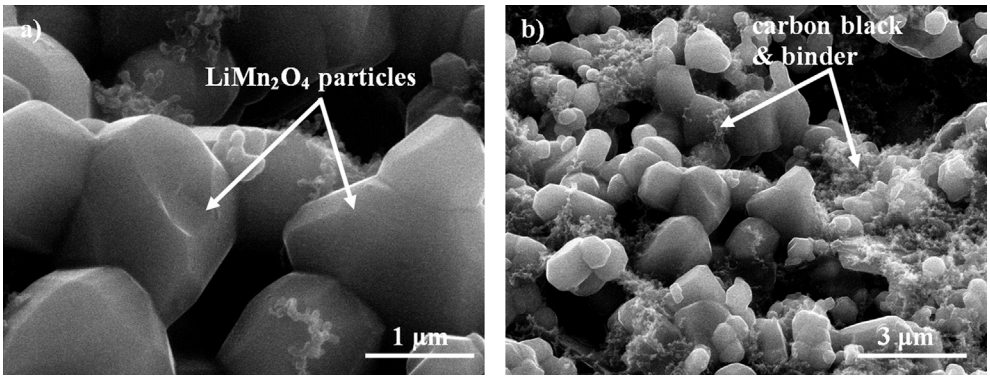

Fig. 4. Top-view SEM images of laser-printed $LiMn_2O_4$ thick films before calendering showing interconnected $LiMn_2O_4$ particles (a) and active particle coating with carbon black/binder (b).

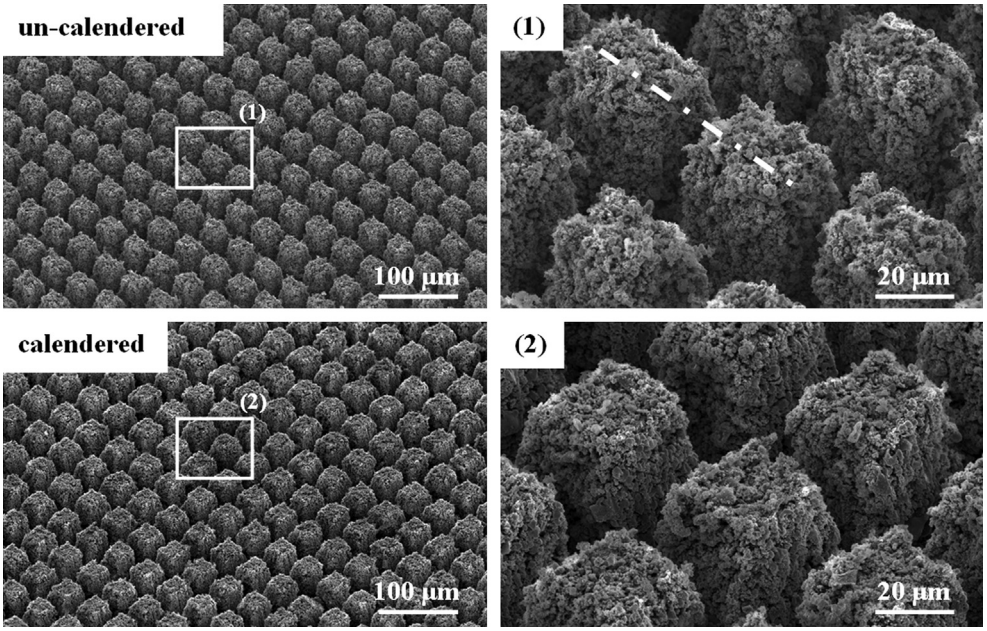

Fig. 5. SEM images of laser-printed and laser structured $LiMn_2O_4$ cathodes. The dotted line indicates exemplarily the scan path for white light profilometry measurement shown in Fig. 6.

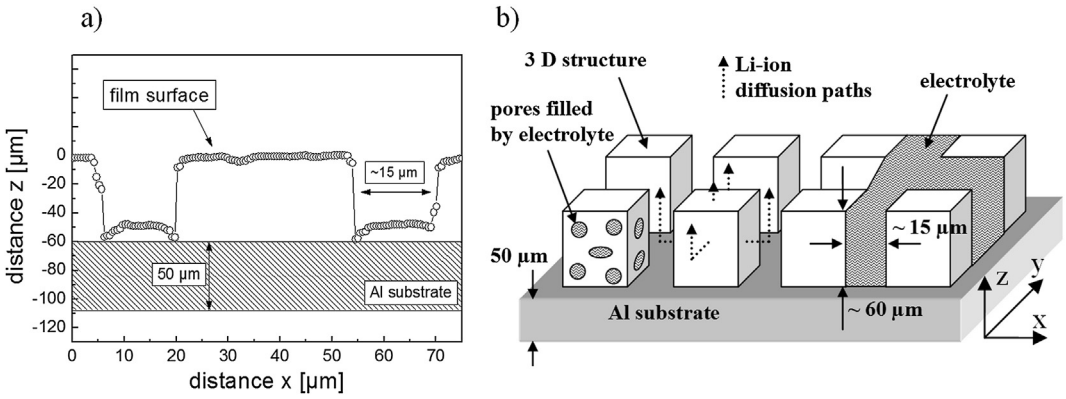

Fig. 6. White light profilometry data (a) and schematic diagram of an array of laser manufactured $LiMn_2O_4$ microstructures in un-calendered films (b) with aspect ratio of channel structures of about 4.

from white light profilometry measurements (Fig. 6, a) over the measuring path indicated by a dotted line in Fig. 5.

These data indicate that a single microstructure has a width of about 35 µm and that the composite material could be ablated almost down to the Al substrate, while the channel width remained about 15 µm (Fig. 6). Laser-printed electrode structures allow multiple and shorter Li-ion diffusion paths, especially out of the bulk material, by allowing the particles in deeper film layers to make direct contact with the liquid electrolyte due to the inherent porosity of the layers [3] (Fig. 6). For laser structured electrodes, the electrolyte distribution is much more uniform and in addition to pores on nm- and µm-scale, laser-induced pores on µm-scale enable the bulk material to be well wetted (Fig. 6). A cross-sectional scheme of how the electrolyte distribution is influenced by a 3 D topography, e.g. for lithium manganese oxide thin films, is described elsewhere [20].

3.3. Electrochemical formation of laser treated $LiMn_2O_4$ thick films

Laser-printed (untreated), calendered, structured and calendered/structured thick films (Fig. 3) featured different active masses m_{active} due to variations in the overall thickness of the electrodes.

The initial conditioning process for all Li-ion cells was carried out using CV measurements (Fig. 7). The 0.02 mV s^{-1} scan rate was used for all experiments and equals a charging and discharging time of about 18 h for each half-cycle. This was estimated to be slow enough for the conditioning process and initial growth of the solid electrolyte interphase (SEI). The oxidation processes of manganese ions take place in the 4 V region indicated by two current peaks at voltages of 4.01 −4.05 V and 4.14−4.18 V, respectively. These observations are in good agreement with the data reported in the literature [21–23] indicating the two-step Li-ion extraction from the cubic host. The reduction processes were observed to occur at 4.07−4.1 V and 3.95−3.98 V while Li-ions are reinserted into the cubic lattice during discharge of the cell. Using CV, the experimentally available capacity was measured and used for calculation of the currents for further C-rate cycling. It was found that the discharge capacities differ as a result of differences in active mass. In addition, the structured cathode exhibited a capacity of 40.0 µAh mg^{-1} (m_{active} = 5.01 mg) for the third discharge cycle which is obviously below the capacity value of 67.4 µAh mg^{-1} measured for a calendered cathode with comparable active mass of m_{active} = 5.22 mg (Fig. 7). The differences in capacity values may be attributed to improved particle contact for the calendered films. Furthermore, the increase in effective surface for a laser structured cathode may promote the amount of SEI formation which is accompanied by the consumption of Li-ions. Advantages of combining the calendering and the structuring process can be estimated from the formation cycle for a calendered/structured film (Fig. 7). Even at slow scan rates, the peak currents of approximately 115−130 µA for oxidation and 90−115 µA for reduction processes are much higher than the peak currents obtained for simply calendered (oxidation: 70−100 µA, reduction: 60−70 µA) or structured films (oxidation: 60−75 µA, reduction: 50−55 µA) with even higher active mass. Finally, the redox couples of calendered/structured cathodes are sharp and well separated indicating that the charge transfer during discharge is nearly completed around 3.7 V, while all other cathodes show reduction reactions and, therefore, charge transfer even below 3.7 V.

3.4. C-rate testing of laser modified $LiMn_2O_4$ thick films

The laser-printed (untreated), calendered, laser structured and calendered/laser structured $LiMn_2O_4$ thick films were electrochemically tested by the galvanostatic method (Fig. 3) after applying the conditioning procedure previously described (Fig. 7). The discharge capacities were normalized for a C/10 discharging rate for evaluating the capacity drop of different battery arrangements, especially at 1 C discharging rate (Fig. 8).

Calendered as well as untreated thick films show slightly higher capacity within the first five cycles at C/10 than structured or calendered/structured films. This may be due to the fact that the increased skin surface of laser-generated 3D structures enhances the reaction area of particles with liquid electrolyte resulting in Li-ion consumption through SEI formation. This formation is known for $LiMn_2O_4$ to be a continuous process [24]. On further cycling, the C-rate was continuously enhanced up to 1 C discharging rate while the charging rate was set to be constant at C/5 (Fig. 8). Calendered thick films exhibited the lowest capacity retention, especially at 1 C discharging rate, compared to all other films. This clearly demonstrates that besides improved electrical contact through calendering, a proper amount of pores filled by liquid electrolyte is necessary for high C-rate cycling while particles in compacted composite films may have their contact with the electrolyte diminished due to their reduced intrinsic porosity. Zheng et al. [25] investigated that the calendering process affects the porosity value of thick films. The capacity value can decrease with reduced porosity due to the fact that the specific area is lowered, hindering the lithium-ion migration [25]. Untreated films show slightly higher discharge capacity than structured films for a C/5 (77% versus 72%) and C/2 rate (67% versus 62%), while the irreversible

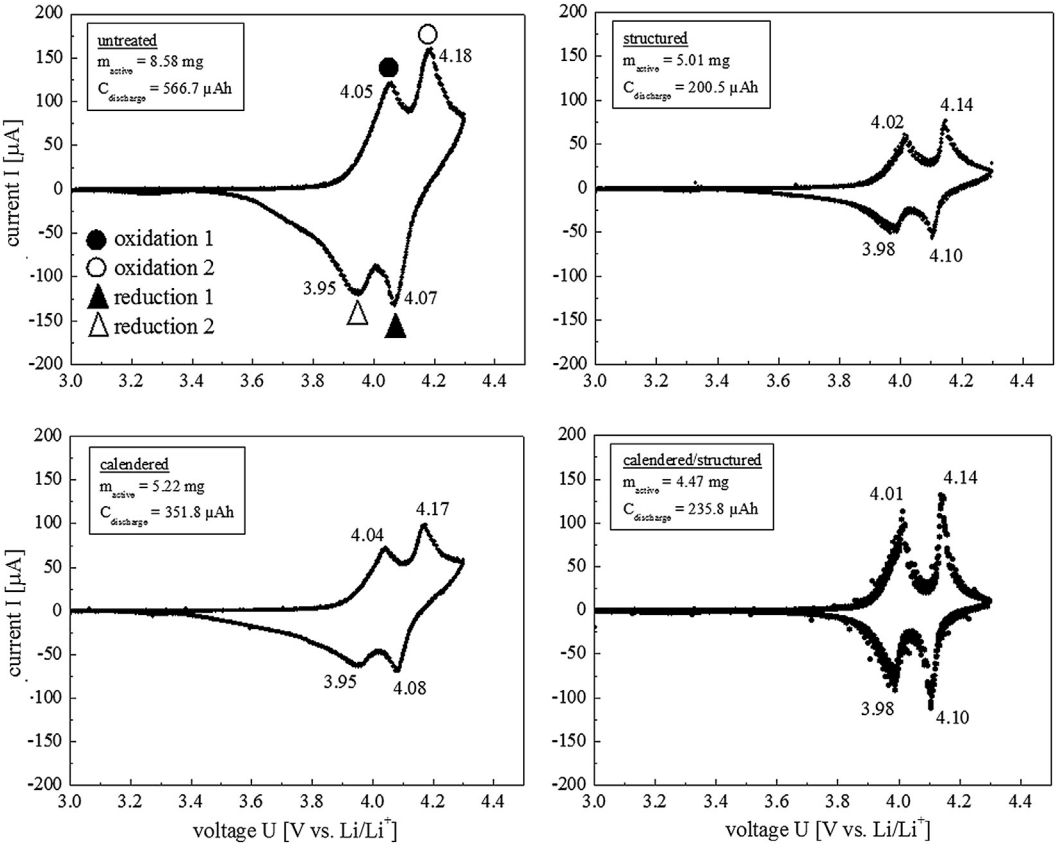

Fig. 7. Cyclic voltammograms obtained at 3rd scan for laser-printed (untreated), calendered, laser structured and calendered/structured $LiMn_2O_4$ thick-film electrodes. The scan rate was set to 0.02 mV s^{-1}.

capacity loss is about 40% for structured and 30% for untreated films when reducing the discharging rate to C/5 after 35 cycles (Fig. 8). The most stable cycling behaviour was observed from the calendered/structured films for all C-rates (C/10 excluded) due to the fact that the calendered/structured films provide both improved electrical contact through calendering and high porosity through laser-generated 3D microstructures. The capacity loss for the calendered/structured cathodes counts 30–33% at 1 C discharge rate, while all other samples show capacity loss of about 48–55% at the same discharging rate. Furthermore, calendered/structured films exhibit an irreversible capacity loss of about 26.4% at a C/5 rate (compared to the 1st discharge) and may be, therefore, promising for long-term cycling at high C-rates. The capacity values [%] for discharge are summarized in Table 2. It is obvious that calendered/structured $LiMn_2O_4$ films exhibit the best high C-rate performance followed by untreated films.

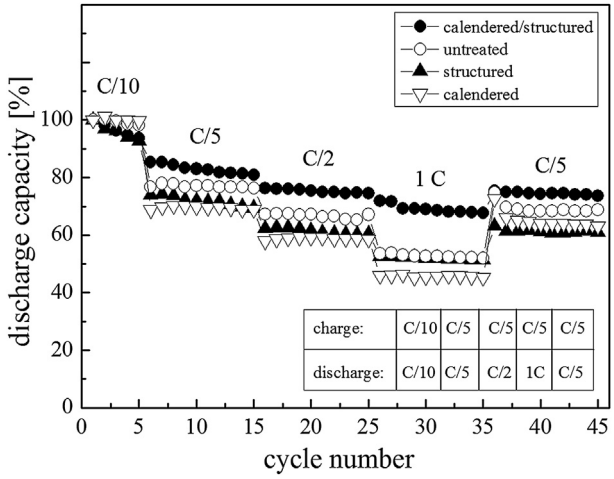

Fig. 8. Normalized discharge capacities for laser-printed (untreated), calendered, laser structured and calendered/laser structured $LiMn_2O_4$ thick-film electrodes. The charging and discharging procedures are listed.

Calendering of laser-printed $LiMn_2O_4$ films seems counterproductive due to the fact that porosity may be reduced to a value at which the electrode cannot soak the electrolyte properly [25] leading to 54.8% capacity loss after 35 cycles (Table 2). With respect to the presented results from CV formation cycles (Fig. 7)

Table 2
Normalized discharge capacity values [%] after 5, 15, 25, 35 and 45 cycles, capacity loss [%] at C/2 (25th cycle) and 1C (35th cycle) testing as well as irreversible capacity loss [%] after 45 cycles for laser-printed (untreated) and subsequent modified (calendered/structured, structured, calendered) $LiMn_2O_4$ thick films.

Cycle number	Calendered/structured	Untreated	Structured	Calendered
	Normalized discharge capacity [%]			
5	93.7	98.1	92.8	99.6
15	80.9	76.4	69.4	68.9
25	74.4	67.1	60.5	58.5
35	67.6	52	51.3	45.2
45	73.6	68.6	60.9	63.2
	Capacity loss [%] compared to 1st cycle			
25	25.6	32.9	39.5	41.5
35	32.4	48	48.7	54.8
	Irreversible capacity [%] loss compared to 15th cycle			
45	9	10.2	12.2	8.3

and galvanostatic testing (Fig. 8), the combination of calendering and laser structuring contributes to the improvement in cycling performance.

3.5. Cell kinetics of cycled $LiMn_2O_4$ thick films

In order to investigate the cell kinetics and reversibility after galvanostatic testing, cycled $LiMn_2O_4$ cathodes were further tested by means of CV measurements. Therefore, the scan rate was enhanced from cycle to cycle which resulted in a steady increase in peak current I_p (Fig. 9). The peak current I_p was plotted versus the square root of the scan rate $\nu^{1/2}$ which is also known as the Randles–Sevcik presentation where $I_p \sim \nu^{1/2}$ [26]. Hence, a linear increase of peak current with enhanced scan rate could be observed for both anodic and cathodic reactions (Fig. 9).

The plotted peak currents for oxidation and reduction reactions in Fig. 9 are characterised and defined in Fig. 7. Furthermore, it should be pointed out that the highest peak currents of oxidation and reduction reactions were determined for untreated and calendered/structured cathodes which are in the same order of magnitude. Peak currents of up to 400 μA were observed for cells with calendered/structured cathodes exhibiting nearly half of active mass compared to untreated cathodes. The peak currents were, moreover, nearly doubled for calendered/structured films in comparison to simply calendered or structured films while the active mass was in the same order of magnitude. This clearly demonstrates the advantages of combining the processes of calendering and laser structuring for improved Li-ion diffusion properties inside the cell and can be explained by the laser-induced increase in skin surface and the model given in Fig. 6. In order to compare reversibility of untreated as well as calendered/structured films, the position of cell voltage is plotted versus scan rate (Fig. 10). Obviously, the voltage positions for oxidation and reduction processes shifted to higher and lower values for an untreated film compared to a calendered/structured film which implicates stronger divergence of redox couples and, therefore, less high C-rate stability. The voltage values of the peak currents for the second oxidation peaks shifted to values above 4.3 V for an untreated film and, hence, it was impossible to detect voltage positions corresponding to a peak current at scan rates >0.14 mV s^{-1}. This implies that laser modified films show cell operation in a proper voltage window which can be maintained even at higher charging and discharging rates.

Furthermore, the voltage positions U of peak currents for both redox couples did not change at 0.02 mV s^{-1} scan rate before and after galvanostatic testing for all films. However, the peak current decreased after decreasing the C-rate again to C/5 in all cases examined, indicating irreversible capacity loss as shown in Fig. 8. Evidence for improved cell kinetics at 1 C discharging rate of calendered/structured cathodes was obtained by plotting the coulomb efficiency [27] versus the cycle number for all samples (Fig. 11). This plot indicates that the structuring process is beneficial for high C-rate cycling of laser-printed and calendered thick films due to a small irreversible capacity loss. While structured and calendered/structured cathodes indicate the highest coulomb efficiencies, the efficiency of the calendered film is below the values for untreated and structured films.

A summary of the results obtained with the four types of $LiMn_2O_4$ films under the various electrochemical tests performed can be found in Fig. 12. The results obtained from CV formation from the 3rd cycle, the capacity loss at the 35th cycle, and the coulomb efficiencies for the 35th cycle (1 C rate) are listed for all battery arrangements. Calendered films exhibited the worst coulomb efficiency value of all battery arrangements which is in good agreement with the observations obtained by the capacity retention values presented in Fig. 8.

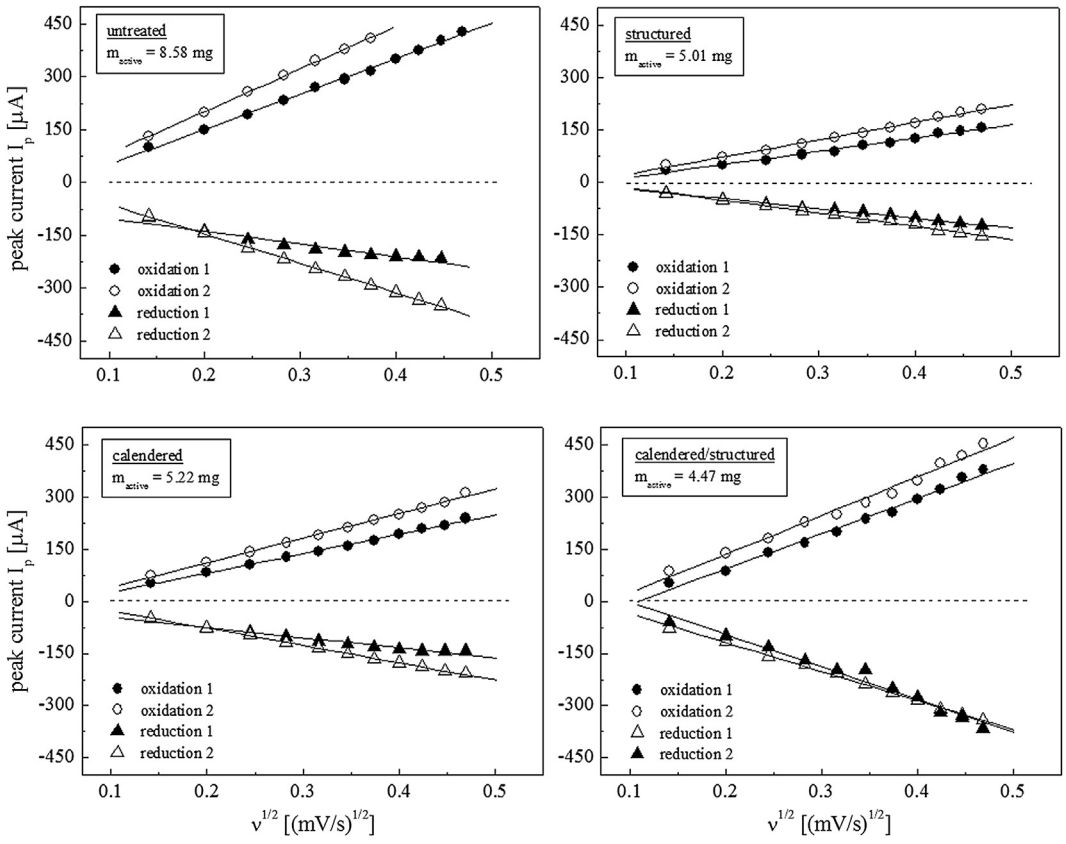

Fig. 9. Peak current I_p vs. the square root of the scan rate $\nu^{1/2}$ for untreated, calendered, structured and calendered/structured $LiMn_2O_4$ thick films.

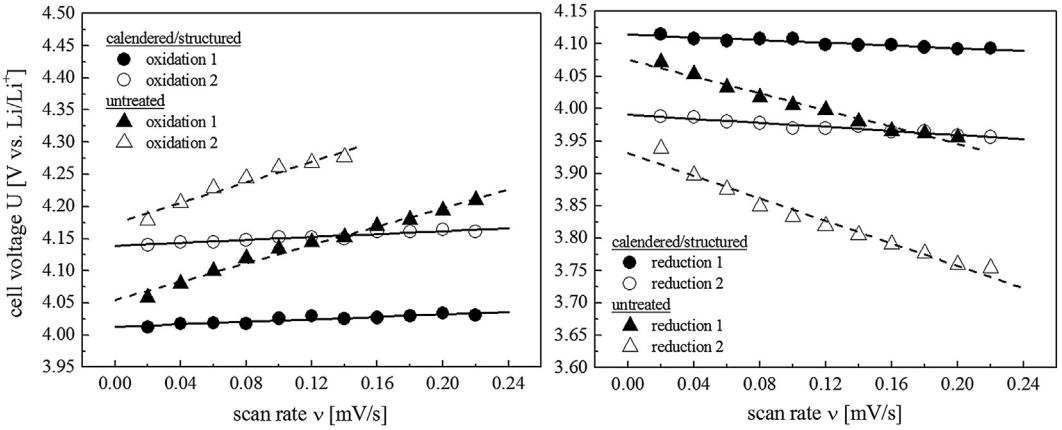

Fig. 10. Cell voltage position U of peak currents for oxidation (left) and reduction processes (right) vs. the scan rate ν for untreated and calendered/structured $LiMn_2O_4$ thick films.

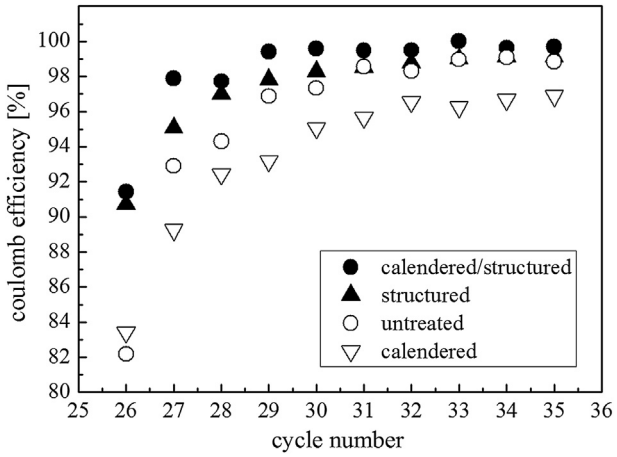

Fig. 11. Coulomb efficiency for untreated, structured, calendered as well as calendered/structured films for ten cycles at C/5 charging and 1C discharging rate.

Regarding the coulomb efficiency, calendered/structured films performed best followed by laser structured, untreated and calendered films (Fig. 12). Calendered cathode films exhibited the overall worst performance, which was found to be due to closure of pores which must be filled with electrolyte. Laser structured cathodes showed good coulomb efficiency due to increased porosity and more efficient Li-ion diffusion pathways. Nevertheless, the low peak currents during CV cycling indicated lowered electron flow compared to calendered films.

4. Conclusions

$LiMn_2O_4$ composite material was laser-printed onto flexible Al substrates for realizing porous thick-film cathodes with thickness of 60 μm. The laser-printed cathode films were calendered and/or laser structured in order to manufacture 3D microstructures with improved electrical contact to the Al substrate and to improve the electrolyte wetting behaviour. The laser structuring process resulted in 3D grid microstructures with an aspect ratio of about ~1.7 and therefore, increased skin surface for enhanced Li-ion diffusion kinetics as was observed by CV and galvanostatic testing. Untreated and calendered/structured films indicated the highest peak currents through electrochemical priming by CV while the peak currents were lower for both calendered or laser structured films with comparable amount of active mass. Furthermore, galvanostatic testing revealed that the calendered/structured cathodes retained about 70% of their initial discharge capacity at a 1 C rate. Therefore, the high C-rate performance could be improved by an array of 3D

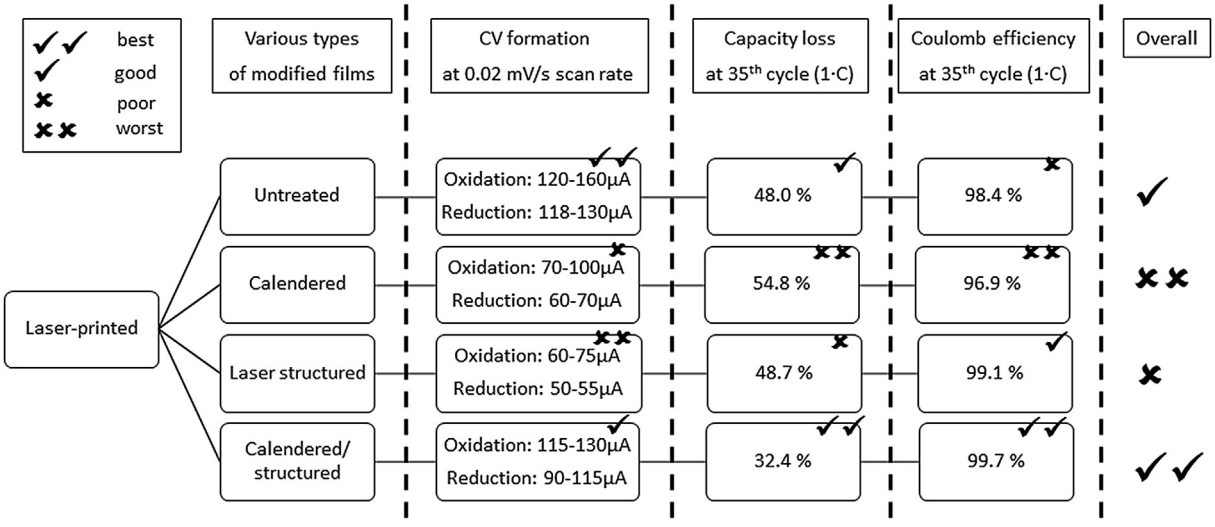

Fig. 12. Flow-chart summarizing the experimental procedure, key results and the overall performance for the laser-printed/laser structured $LiMn_2O_4$ thick films.

grid rectangular structures in combination with pre-calendering compared to untreated, calendered or laser structured films. Electrochemical cycling of the calendered/structured cathode exhibited less degradation as was found by reducing the C-rate from 1 C to C/5 as well as by post-cycling using CV with variable scan rates. This improvement resulted from a combination of increased electrical contact due to calendering as well as enhanced Li-ion diffusion paths due to laser-induced enhanced porosity and improved electrode wetting. Finally, laser-printing as well as laser structuring can be performed on small footprint areas and with high processing speeds. Therefore, these processes might be suitable for manufacturing of complete solid-state 3D microbatteries with improved cycling performance as well as for up-scaling and process transfer to large areal electrodes as required, e.g. for pouch cell manufacturing where calendering techniques and proper electrolyte filling are essential manufacturing steps.

Acknowledgments

We are grateful to our colleague H. Besser for his technical assistance during laser material processing. We gratefully acknowledge the financial support by the Helmholtz Association in frame of the programme “Science and Technology of Nanosystems” and “Helmholtz-Portfolio” about reliability and integration of battery systems. Finally, the support for laser processing by the Karlsruhe Nano Micro Facility (KNMF, http://www.knmf.kit.edu/) a Helmholtz research infrastructure at the Karlsruhe Institute of Technology (KIT) is gratefully acknowledged. H. Kim and A. Piqué were supported by the Office of Naval Research (ONR) through the Naval Research Laboratory Basic Research Program.

References

[1] Y.M. Lin, H.C. Wu, Y.C. Yen, Z.Z. Guo, M.H. Yang, H.M. Chen, H.S. Sheu, N.L. Wu, J. Electrochem. Soc. 152 (2005) A1526–A1532.
[2] D.K. Kim, P. Muralidharan, H.W. Lee, R. Ruffo, Y. Yang, C.K. Chan, H. Peng, R.A. Huggins, Y. Cui, Nano Lett. 8 (2008) 3948–3952.
[3] H. Kim, R.C.Y. Auyeung, A. Piqué, J. Power Sources 165 (2007) 413–419.
[4] J.W. Long, B. Dunn, D.R. Rolison, H.S. White, Chem. Rev. 104 (2004) 4463–4492.
[5] B.J. Hwang, C.Y. Wang, M.Y. Cheng, R. Santhanam, J. Phys. Chem. C. 113 (2009) 11373–11380.
[6] J.L. Li, C. Daniel, D. Wood, J. Power Sources 196 (2011) 2452–2460.
[7] A. Piqué, C.B. Arnold, H. Kim, M. Ollinger, T.E. Sutto, Appl. Phys. A 79 (2004) 783–786.
[8] C.B. Arnold, P. Serra, A. Piqué, MRS Bull. 32 (2007) 23–31.
[9] R. Wartena, A.E. Curtright, C.B. Arnold, A. Piqué, K.E. Swider-Lyons, J. Power Sources 126 (2004) 193–202.
[10] H. Kim, J. Proell, R. Kohler, W. Pfleging, A. Piqué, J. Laser Micro/Nanoen. 7 (2012) 320–325.
[11] K. Sun, T.-S. Wei, B.Y. Ahn, J.Y. Seo, S.J. Dillon, J.A. Lewis, Adv. Mater. 25 (2013) 4539–4543.
[12] J. Proell, R. Kohler, A. Mangang, S. Ulrich, C. Ziebert, W. Pfleging, J. Laser Micro/Nanoen. 7 (2012) 97–104.
[13] J. Pröll, R. Kohler, M. Torge, S. Ulrich, C. Ziebert, M. Bruns, H.J. Seifert, W. Pfleging, Appl. Surf. Sci. 257 (2011) 9968–9976.
[14] R. Kohler, J. Proell, S. Ulrich, V. Trouillet, S. Indris, M. Przybylski, W. Pfleging, Proc. SPIE 7202 (2009) 720207, http://dx.doi.org/10.1117/12.809164.
[15] R. Kohler, P. Smyrek, S. Ulrich, M. Bruns, V. Trouillet, W. Pfleging, J. Optoelectron. Adv. Mater. 12 (2010) 547–552.
[16] R. Kohler, H. Besser, M. Hagen, J. Ye, C. Ziebert, S. Ulrich, J. Proell, W. Pfleging, Microsyst. Technol. 17 (2011) 225–232.
[17] R. Kohler, J. Proell, M. Bruns, S. Ulrich, H.J. Seifert, W. Pfleging, Appl. Phys. A 112 (1) (2012) 77–85.
[18] A. Slocombe, A. Taufik, L. Li, Appl. Surf. Sci. 168 (2000) 17–20.
[19] A. Slocombe, L. Li, Appl. Surf. Sci. 154 (2000) 617–621.
[20] J. Pröll, R. Kohler, M. Torge, M. Bruns, M. Przybylski, S. Ulrich, H.J. Seifert, W. Pfleging, Proc. SPIE 8244 (2012) 82440S, http://dx.doi.org/10.1117/12.906714.
[21] T. Fukutsuka, K. Sakamoto, Y. Matsuo, Y. Sugie, T. Abe, Z. Ogumi, Electrochem. Solid-State Lett. 7 (2004) A481–A483.
[22] J. Xie, K. Kohno, T. Matsumura, N. Imanishi, A. Hirano, Y. Takeda, O. Yamamoto, Electrochim. Acta 54 (2008) 376–381.
[23] C.J. Curtis, J.X. Wang, D.L. Schulz, J. Electrochem. Soc. 151 (2004) A590–A598.
[24] K. Edström, T. Gustafsson, J.O. Thomas, Electrochim. Acta 50 (2004) 397–403.
[25] H.H. Zheng, L. Tan, G. Liu, X.Y. Song, V.S. Battaglia, J. Power Sources 208 (2012) 52–57.
[26] P.C. Howlett, D.R. MacFarlane, A.F. Hollenkamp, Electrochem. Solid-State Lett. 7 (2004) A97–A101.
[27] J.P. Wang, B.G. Cao, Q.S. Chen, F. Wang, Control Eng. Pract. 15 (2007) 1569–1576.